Electronic structure study of ion-implanted Si quantum dots in a SiO_2 matrix: Analysis of quantum confinement theories

E. G. Barbagiovanni,* L. V. Goncharova, and P. J. Simpson
Department of Physics and Astronomy, University of Western Ontario, London, Ontario, Canada, N6A 3K7
(Received 24 July 2010; revised manuscript received 30 September 2010; published 13 January 2011)

The electronic states and optical properties of Si quantum dots (QDs) with variable size prepared by ion implantation in a SiO_2 matrix are studied by x-ray photoemission spectroscopy (XPS), photoluminescence (PL), and Raman spectroscopy. The results are compared with several theories of quantum confinement. Our Si 2*p* binding energies and the valence band energies do not change as a function of QD diameter nor compared to the bulk Si values. Raman spectra show no signs of stress on the Si-QDs. XPS data indicates the presence of a Si_2O_3 interfacial layer between the Si-QDs and the surrounding SiO_2 matrix, which is understood to relieve stress in the QDs and to cause pinning of the valence level. Our XPS results for ion-beam implanted QDs are compared with other group's studies for Si-QDs prepared by alternative methods, and discrepancies in the interfacial compositions are discussed. These results call into question the fundamental predictions and assumptions of many quantum confinement models. It is concluded that the lack of a shift in the valence band is due to a symmetry-breaking process in the hole states, which is not currently accounted for by theory, demonstrating the importance of the hole states during radiative events. This work is intended as a first step in highlighting the features that should be present in a theoretical formalism for embedded Si-QDs, and cause is given to abandon particular formalisms.

DOI: 10.1103/PhysRevB.83.035112 PACS number(s): 78.67.Hc, 73.21.La, 73.22.−f, 61.46.Hk

I. INTRODUCTION

Mesoscopic semiconductor structures embody an extensive array of research with applications in electronic and optoelectronic devices and in the physical sciences.[1] Research into mesoscopic structures is an active field focused on fundamental physics at the nanoscale through the study of phenomena such as the Kondo effect, Andreev reflections, and spin qubits (for a concise review of these topics, see Ref. 2). Despite the active research into higher order effects, there remains a lack of a complete understanding of the low-dimensional electronic structure, which is particularly true for mesoscopic systems formed by ion-implanted quantum dots (QDs). Part of the difficulty arises from the fact that low-dimensional theories rely heavily upon the mathematics of the bulk system. Therefore, the range of effects due to lowered dimensionality are masked through the transference of bulk properties to the low-dimensional case. For example, the difficulty in predicting the electronic structure is in the correct choice of the wave states. The breaking of **k**-selection rules with diminishing QD size indicates that using a Bloch-wave multiple in the basis set is a questionable assumption, as clearly demonstrated in cohesive energy methods that search for overlaps in the Bloch states with the crystal potential.[3] *Ab initio* characterization of quantum confined structures is not possible at present, albeit semiempirical methods are relatively well established.[4] Because of the connection between the electronic and optical states, extensive research has been dedicated to the optical properties in low-dimensional structures. Several possibilities for the mechanism of radiative recombination have been proposed and are under debate,[5] while zero-dimensional (0D) Si and/or Ge structures as direct or quasidirect gap materials have yet to be established. For a concise overview of the mechanisms involved in confined nanostructures, see, for example, Refs. 6–8. Of the various mechanisms for radiative recombination, quantum confinement is accepted as the correct theory for describing *direct* electron-hole recombination efficiency in nanostructures,[6] albeit there are many versions of this theory, which can simultaneously fit experimental data. The phenomenon of quantum confinement allows one to overcome the difficulty in obtaining high radiative efficiency in a semiconductor material, which is a function of the interband coupling efficiency. For direct gap materials, radiative processes can occur without phonon coupling. One increases the efficiency of the radiative process with nanostructured materials (or artificial atoms) because of the creation of discrete energy levels when at least one dimension of the system is less than or equal to the exciton Bohr radius. For indirect gap materials, low radiative efficiency is particularly challenging, because one needs a phonon to ensure momentum conservation is maintained. On the other hand, a nanostructured material avoids this problem by increasing the probability of wave function overlap between the electron and hole states, therefore breaking the **k**-selection rules and implying indirect gap materials can radiate without phonon assistance.[9] Hence, the radiative efficiency is substantially larger in nanostructured materials (for direct and indirect materials), which is why there is strong interest in these systems. Experimentally, the theory of quantum confinement states that if the confinement dimension of a nanostructure is decreased, the peak photoluminescence (PL) energy is increased. Other possible sources for radiative events are through defect or interface states. However, these states do not have an associated size dependence; therefore, it is possible to distinguish between different radiative mechanisms.[6,8] In addition, defect-related PL is in the blue-green energy band, while quantum confined PL is in the red energy band. As pointed out by Zdetsis, the discrepancy between theoretical and experimental results in this field is significant.[10] There

are several reasons why this is the case. Experimentally, QD growth conditions may be controlled only to a limited extent; for example, there may be oxygen contamination. Theoretically, fitting of empirical parameters and exchange and correlation effects are inadequately approximated in calculations. For instance, if one employs density functional theory (DFT), determination of the electronic density of states (DOS) requires knowledge of the electronic wave states. There are several ways to pick these states; Zdetsis *et al.*[10] use a multireferenced second-order many-body perturbation theory, Ramos *et al.*[11] use projector augmented waves, and Nguyen *et al.*[12] use pseudopotentials established through geometric convergence. Specifically, Nguyen *et al.* demonstrated that one does not expect any change in the valence level DOS; however, they calculate a gap energy E_G too large (3.1 eV) for embedded Si-QDs (e-Si-QDs).[12] While linear combinations of atomic orbital methods yield results that have a stable valence band (VB) energy, as expected from the assumptions of the theory, nonetheless, the results do not fit experimental data for e-Si-QDs.[13] Furthermore, tight-binding methods, which are in extensive use, also require information about the electronic wave states. In one case, the Hückel-type nonorthogonal tight-binding method is used and the results fit well with experimental data for porous Si.[14] In another approach, transferable adjustable parameters are used and no good fit with experimental results is established.[15] On the other hand, "particle-in-a-box" type calculations assume perfect symmetry between the electron *e* and hole *h* states. In these calculations, the *h* term gains a dimensional dependence, which leads to an artificially large expansion of E_G. In previous work, we demonstrated that an *ab initio* field theoretical formalism must restrict the confining potential to one dimension for the calculated band-gap values to fit the experimental PL results.[16] However, a one-dimensional (1D) confining potential is not correct since transmission electron micrographs (TEM) reveal e-Si-QDs as structures with three-dimensional (3D) confinement.[17] To overcome this challenge, researchers have applied variational[18] or pseudopotential techniques,[19] which yield variations in the dimensional dependence as $E_G \propto \frac{1}{D^n}; n \in \mathbb{Q}^+$. One must further consider the preparation technique, in and of itself, which affects the resulting PL through the introduction of defect states and/or varying interface states. For example, ion implantation introduces defects during the implantation process, which are subsequently annealed.[20] The radiative properties for ion-implanted nanostructures are further controlled by the surrounding matrix,[21] implantation dose, thermal budget, the gas environment during annealing, and implantation energy, to name a few.[22] For example, in the work of Shimizu-Iwayama *et al.*, Si nanoclusters formed by ion implantation are shown to exhibit variation in the peak PL energy with implantation dose, which the authors attribute to the effect of quantum confinement.[23] Further, in this same work, the authors find that by varying the annealing time from $1 \rightarrow 8$ h, there is no change in the peak PL energy. As we stated previously, the lack of change in PL should correspond to no change in the nanocrystal diameter. However, the authors assume that prolonged annealing does not change the number of nanocrystals but instead causes an increase in the mean diameter. In contrast, Garrido *et al.* shows that the mean nanocrystal diameter does not change with prolonged annealing, as expected under the hypothesis of Ostwald ripening.[24] The role of O_2 during annealing on the radiative process is also explored by Shimizu-Iwayama *et al.*, which fixes the PL energy to the value of disordered Si at 1.7 eV.[23] Si or Ge QD formation using ion implantation followed by thermal annealing is a promising technique for incorporation of QDs into a dielectric film. TEM studies can establish the crystal structure of e-Si-QDs experimentally as diamondlike (high-quality TEM images are shown in Refs. 25 and 26, where the crystallinity of the e-Si-QDs is clearly seen; however, the boundary with the matrix is not clear). Because of their low impurity content, these systems are ideal for studying fundamental physical models. On the other hand, characterization of the electronic structure of QDs in a dielectric material is a nontrivial task, because the object of study is embedded in a surrounding matrix. Therefore, most studies of the optical and electronic properties use QDs created by methods other than ion implantation. For example, it has been considered that e-Si-QDs in a dielectric material (particularly, SiO_2) have properties similar to porous Si.[27,28] This approximation is not well founded, considering the difference in PL results for porous Si: diameter of $D = 1.76$ nm corresponds to a peak wavelength of $\lambda_{peak} = 705$ nm, versus e-Si-QDs: $D = 1.78$ nm corresponds to $\lambda_{peak} = 883$ nm.[16,29] Moreover, e-Si-QDs prepared by techniques other than ion implantation have different structural properties and interface composition, which potentially implies differences in the carrier recombination dynamics. For instance, e-Si-QDs formed by deposition of Si-rich SiO_2 films via a plasma-enhanced chemical vapor deposition (PECVD) process followed by thermal annealing yield all four Si oxidation states.[30] As a result, PECVD-QDs have a significant number of defect centers resulting in numerous charge-trapping centers. These considerations imply the need for a more detailed understanding of the electronic states as a function of reduced dimension, both experimentally and theoretically, to quantitatively distinguish the various radiative mechanisms. This article attempts to juxtapose various methods and ideas in order to exemplify key features of e-Si-QDs. In this article, we study the electronic structure of e-Si-QDs experimentally and theoretically. Experimentally, we measure the x-ray photoemission spectroscopy (XPS) spectra of e-Si-QDs of varying size, focusing on the Si 2*p* state and the valence-level DOS. We obtain structural information on the e-Si-QDs by looking at the Raman spectra, especially at the shifts due to stress. Theoretically, we compare structural predictions made by molecular dynamics (MD) simulations by other groups against our XPS results, with respect to the suboxide layer surrounding the QD and stress. The valence levels are further analyzed theoretically by noting predictions about the hole contribution to quantum confinement. To summarize, we compare our results with published results and argue that QDs made by methods other than ion implantation cannot be compared to ion-implanted-e-Si-QDs, as is typically done in the literature.

II. EXPERIMENT

Si^- ion implantation was carried out at 95 keV into 280-nm thermally grown oxide (Silicon Sense) at four different doses: 8.5×10^{16}, 9.0×10^{16}, 9.5×10^{16}, and 1.0×10^{17} cm^{-2},

labeled a, b, c, and d, respectively. These conditions place the center of the implant profile ≈140 nm deep, according to the stopping and range of ions in matter (SRIM) program and experimentally observed in TEM.[31] The implantation was performed at room temperature under normal incidence and a vacuum of 10^{-7} torr. The samples were then annealed in a tube furnace all under the same conditions of 1100°C, 120 min in a N_2 flow. The furnace was pumped down to ≈25 mTorr prior to annealing to remove possible contaminants. Without being exposed to air, the samples were subsequently annealed at 500°C in forming gas (N_2/H_2, 95% N_2) for 60 min.

PL measurements were performed at room temperature with a 325-nm laser at 17 mW and an effective power density of 0.64 W/cm^2. Light emission was analyzed by an Ocean Optics spectrometer with 600 gratings/mm, resulting in a large spectral window of 350–1000 nm.

In previous studies, it was established that the Si-QDs are located roughly 95 nm below the surface after annealing, following diffusion from the implant depth of 140 nm.[16,20] Therefore, for the samples a, b, c, and d approximately 90 nm of the surface SiO_2 was removed using a 4:1 buffer HF solution (as determined by ellipsometry) for XPS. A reference sample (Si-ref) was prepared by etching the ultrathin native oxide layer with HF. A SiO_2 reference (SiO_2-ref) sample was also prepared using the same thermal oxide of 280 nm, but with no implantation performed, and it was etched by an amount similar to that of the four samples, thus eliminating any possibility that the differences in surface chemistry between samples arise solely due to the HF process.

The XPS analyses were carried out with a Kratos Axis Ultra spectrometer using a monochromatic Al K(α) source (15 mA, 14 kV) at Surface Science Western. The instrument work function was calibrated to give a binding energy (BE) of 83.96 eV for the Au $4f_{7/2}$ line for metallic gold, and the spectrometer dispersion was adjusted to give a BE of 932.62 eV for the Cu $2p_{3/2}$ line of metallic copper. High-resolution analyses were carried out with an analysis area of 300 × 700 μm and a pass energy of 20 eV. Spectra have been charge corrected to the main line of the C 1s peak (adventitious carbon) set to 284.8 eV. Spectra were analyzed using CasaXPS software (version 2.3.14).[32] The micro-Raman system consists of holographic optics, a single (1800 groove/mm) grating, 0.5-m spectrometer, and a liquid-nitrogen-cooled charge-coupled device (CCD) detector (1100 × 330 pixels), with a resolution of ±1 cm^{-1}.

A. Analysis of HF procedure

The nature of this experiment is evidence that characterizing e-Si-QDs is technically challenging as one may rightly question the validity of the use of HF in the XPS results. Here we argue briefly that while the technique is not entirely satisfying, it is the best method available currently and does provide confident results. First, we mention that an alternative technique is to use Ar sputtering to bring the e-Si-QDs with the depth resolution of XPS (typically 3 → 5 nm); however, this technique suffers from differential sputtering of O (4:1 Ref. 31); therefore, suboxide results are questionable.[26,33] One could also produce e-Si-QDs using a shallow implant condition; we argue in Sec. IV A that this technique produces a structurally different e-Si-QD and should not be compared to our work.

One must consider whether the process of using HF to remove surface layers of SiO_2 will also etch the e-Si-QDs. It is known that HF preferentially acts on SiO_2, but it can also etch Si, albeit at a much slower rate.[34] In the work of Hundertmark, he shows, by the use of AFM imaging techniques, that the e-Si-QDs remain on the surface of the substrate after a sufficiently long etch.[34] Furthermore, Hundertmark demonstrates that peak PL energy of the etched samples does not shift significantly, meaning there is no substantial change in the diameter of the e-Si-QDs. At the same time, there is a reduction in the PL intensity, which is expected because some e-Si-QDs eventually are removed from the sample.

The next question to consider is whether the HF process will create artificial suboxide peaks in the XPS data. In the work of Brongersma *et al.*, it was shown that the etch rate is significantly reduced when the HF solution is in the vicinity of the e-Si-QDs and not before, a result we also observed in earlier test samples.[35] This result is an indication that the etchant is reacting with a suboxide state and does not preferentially etch that state, as compared to the SiO_2 matrix. Therefore, if the HF etching process is discontinued before the etchant is in the vicinity of the e-Si-QDs (evident in a differing etch rate), then one can be confident that the as-formed e-Si-QDs from the annealing procedure remain and have the same suboxide state. Furthermore, we continuously monitored the thickness of removed SiO_2 layers by the use of ellipsometry (10-s etch between measurements) to ensure we did not etch the QDs. Hence, our XPS results probe a couple nanometers of undamaged e-Si-QDs with any error in the measurements arising from the surface monolayer of the sample.

III. RESULTS

Experimentally measured PL peak wavelength positions for samples a–d are shown in Table I. Note that a full-width half maximum (FWHM) of ≈150 nm is observed for all samples. There is a 40-nm shift in the PL peak wavelength from samples a to d. As discussed in Sec. I, several models for quantum confinement have been used to fit experimental data, including our previously published 1D model.[16] Therefore, it is prudent to first establish a Si-QD diameter comparison. Using the various theoretical models described in the following paragraph, the QD diameter is calculated using our experimental peak PL energy in Table I, thus illustrating the large variation between theories. Improvements to the theory are represented in Fig. 1 and discussed in detail later.

The work of Delerue *et al.* has been applied to many studies of e-Si-QDs, and therefore it serves as a good comparison.[36–41] Delerue *et al.* establish

$$E_{\mathrm{PL}} = E_{\mathrm{Gap}}(\infty) + \frac{3.73\ \mathrm{eV}\cdot\mathrm{\AA}}{D^{1.39}}, \tag{1}$$

where $E_{\mathrm{Gap}}(\infty)$ is the bulk gap energy of 1.12 eV, D is the diameter, and E_{PL} is the peak energy of the PL spectrum. However, the calculation in that work is for porous Si, which does not apply to the case of embedded QDs.[42] In the

TABLE I. Photoluminescence peak maxima and respective calculated QD diameters.

Sample	λ_{peak} (nm)	E_{PL} (eV)	Barbagiovanni *et al.* [Eq. (3)] Diameter (nm)	Ramos *et al.* [Eq. (2)] Diameter (nm)	Delerue *et al.* [Eq. (1)] Diameter (nm)
a	830	1.49	1.55	8	2.5
b	850	1.46	1.62	8.7	2.8
c	862	1.44	1.67	9.3	3.0
d	870	1.42	1.72	9.9	3.3

work of Ramos *et al.* (for e-Si-QDs), a different relation is established:[11]

$$E_{PL} = E_{Gap}(\infty) + \frac{29.6\ \text{eV}\cdot\text{Å}}{D}. \quad (2)$$

In our work, we establish[16]

$$E_{PL} = E_{Gap}(\infty) + \frac{89.2\ \text{eV}\cdot\text{Å}^2}{D^2} \quad \text{(1D confinement)}. \quad (3)$$

The results of QD diameter calculations using Eqs. (1), (2), and (3) substituting our experimental peak PL energy for E_{PL} are given in Table I. Notice that each method gives very different QD sizes and size ranges for a single set of experimental data. Because of challenges in determining the diameter of e-Si-QDs experimentally, the accuracy of each method is difficult to establish. More details of our calculation are given in the appendix.

There have been a limited number of studies for ion-implanted e-Si-QDs using XPS.[8,26,33,43,44] A direct comparison of these results is nontrivial since each author uses a different method to determine the QD diameter. In addition, determination of QD size by TEM is limited by the resolution of TEM because of the poor contrast between the e-Si-QDs and the surrounding SiO_2 matrix (typically not better than 1 nm).[25]

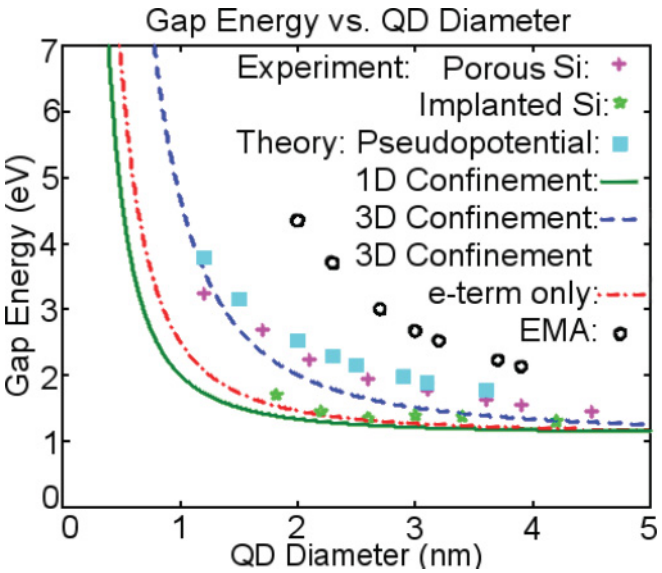

FIG. 1. (Color online) Band-gap variation as a function of particle size. Porous Si, pseudopotential, and effective mass approximation (EMA) from Refs. 4 and 19; implanted Si from Ref. 20; and 3D confinement, 3D confinement *e* term only, and 1D confinement from Ref. 16 (details in appendix).

A further complication arises from the fact that accurate size statistics for QDs in the range of $2 \rightarrow 4$ nm are difficult to obtain, depending on the implantation dose one uses.[26] Meanwhile, determining QD size by scattering experiments is an indirect method. Figure 1 gives the variation of gap energy for samples prepared by ion implantation and for porous Si compared with various theoretical methods. Note that our calculation fits the experimental data the best for e-Si-QDs, where the size is determined using TEM. The details of the calculations used for the curves 3D confinement, 3D confinement *e* term only, and 1D confinement are given in the appendix.

XPS spectra for the samples with varying QD size and the two reference samples are presented in Fig. 2. Spectra were fitted using CasaXPS by fixing the oxidation states of Si^{n^+} ($n = 1,2,3,4$) to the standard shifts with respect to Si^{0^+}, at $+0.9$, $+1.75$, $+2.5$, and $+3.9$ eV for $n = 1,2,3,4$.[45,46] Using Shirley background, Gaussian-Lorentzian line shapes and a branching ratio of 2:1 for Si $2p_{3/2}$ to Si $2p_{1/2}$ with a spin-orbit split of 0.6 eV yielded a fit for only the 0^+, 3^+, and 4^+ as can be seen in Fig. 3. The FWHM for the Si $2p_{3/2}$ peak for 0^+ is 0.47 eV for Si-ref and 0.97, 1.05, 1.02, and 1.08 eV for samples a, b, c, and d, respectively. Figure 3 shows a representative result of this fitting procedure for sample c.

As mentioned in Sec. II, the spectra are charge corrected to the main line of C 1*s* at 284.8 eV; however, there is an

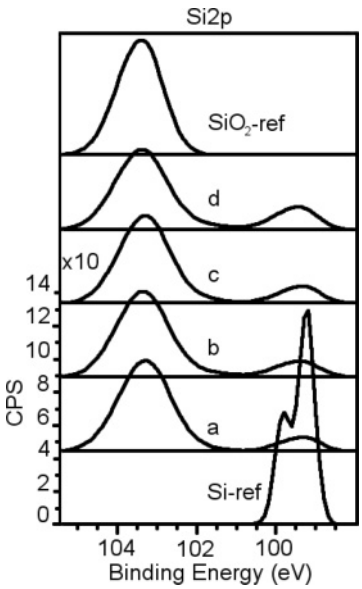

FIG. 2. XPS counts per seconds (CPS) vs binding energy data for Si 2*p* comparison between samples, Si-ref and SiO_2-ref, after charge correction and normalization.

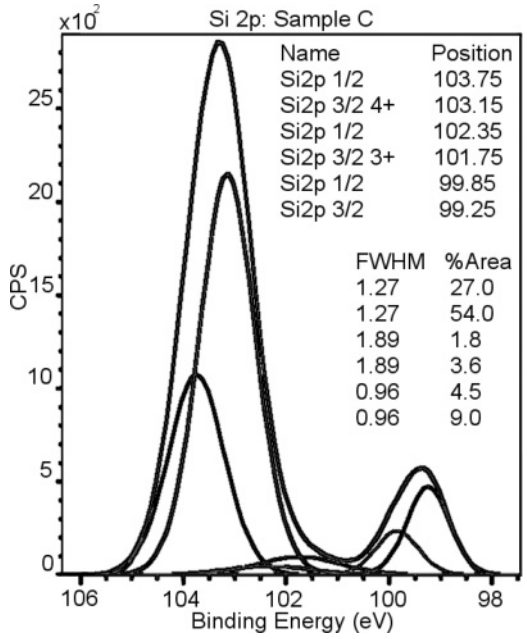

FIG. 3. XPS counts per seconds (CPS) vs binding energy data for Si 2*p* fit for sample c: Oxidation states labeled in legend.

associated error with this process of $\pm 0.1 \rightarrow 0.2$ eV.[47] In our case, we see a significant shift in the C 1*s* peak from our Si-ref and SiO_2-ref peak to the various samples analyzed before the charge correction was applied, as shown in Table II. Comparing the FWHM of C 1*s* in the Si-ref sample at 1.14 eV to sample d, per se, at 1.36 eV, we see a broadening of the peak (samples a, b, and c have similar values). Since the C 1*s* peak is an artifact of contamination from the XPS machine itself, it is instructive to note that the Si-ref sample was loaded into the XPS chamber by a different method than all other samples. The Si-ref sample was cleaned with HF just prior to analysis, and to avoid regrowing the native oxide layer, the sample was loaded through a glove box in an Ar environment; hence the level of contamination was reduced, leading to the differences in the C 1*s* peaks. Furthermore, we do not see charging as a function of QD size.

Table III lists the values for the Si $2p_{3/2}$ peak in the 0^+ and 4^+ state before and after charge correction, also shown in Fig. 2. There is no shift in the Si 2*p* peak as a function of QD size. Note: For the remainder of this paper, analysis is given for charge-corrected peaks.

IV. DISCUSSION

We first note the increase in the FWHM for the Si 2*p* peak from Si-ref to the samples containing Si-QDs; see Table III. This increase is typically attributed to three factors: structural disorder, phonon broadening, and core-hole lifetime.[46] It is well known that e-Si-QDs are crystalline as evident in previously performed TEM imaging (see Sec. I) and as predicted by MD simulations (see Sec. IV B). Therefore, we rule out broadening due to disorder. Significant disorder also leads to stress, and we do not see this effect in Raman results (see Sec. IV B 1). Hence, we can attribute the broadening to both phonon and core-hole effects, which are both observed for Si-QDs; see references within Ref. 46. Furthermore, the core-hole effect is attributed to a dielectric screening effect between the SiO_2 matrix and the e-Si-QDs, which is expected to change as a function of Si-QD diameter.[46] This effect is expected to be on the order of ≈0.5 eV, which is consistent with the broadening that we observe.[43]

TABLE II. XPS C 1*s* peaks (eV), before charge correction.

Si-ref	a	b	c	d	SiO_2-ref
284.99	282.31	282.35	282.27	282.22	286.16

TABLE III. XPS Si $2p_{3/2}$ peaks (eV) charge states 0^+ and 4^+, corrected and uncorrected.

	Si-ref	a	b	c	d	SiO_2-ref
FWHM 0^+	0.47	0.97	1.05	1.02	1.08	
0^+	99.43	96.75	96.85	96.72	96.75	
0^+(corrected)	99.24	99.23	99.30	99.25	99.34	
4^+		100.65	100.75	100.62	100.65	104.61
4^+(corrected)		103.13	103.20	103.15	103.24	103.25

From Sec. III, we see that after charge correcting to the C 1*s* peak and properly accounting for differences in charging between samples, the Si $2p_{3/2}$ peak for both 0^+ and 4^+ exhibits no shift in BE with respect to the reference samples, within experimental error; see Table III and Fig. 2. This is a very important result in understanding the effects of QD size on the low-dimensional electronic structure and deserves a detailed analysis. Primary factors that can cause a shift in the Si 2*p* peak are charging effects, stress (lending to a stretching or contraction of bond length), and quantum confinement effects. The latter is the most important contribution to understand as it gives us detailed insight into quantum confinement theories.[48]

We do not find charging to be a substantial effect and mention it only briefly. Charging is Coulombic where the QDs act as capacitors in a dielectric material.[43] For the case of the largest QD (3 nm), this effect is on the order of ≈0.1 eV, which is not detectable and varies as $\frac{e^2}{2C}$; $C = 4\pi\epsilon_0\epsilon_D D$. Before discussing stress and quantum confinement effects, we present a review of other works on Si 2*p* photoemission studies for QDs.

A. Si 2*p* comparison

Chen *et al.* performed a low-energy implantation (1 keV) into 30 nm of thermally grown oxide.[43] The samples were then annealed for various times in N_2 with no H passivation of dangling bonds, resulting in a range of Si-QD size from 2.5 to 3 nm (estimated by x-ray diffraction). A low-energy implant leaves the Si implant concentration peak near the vacancy peak.[31] This fact means that during the annealing process Si-QDs are forming in a region of high defect concentration, and in turn the formation of stoichiometric oxide is retarded, meaning a higher concentration of suboxide states will remain, as compared to higher energy implanted samples. Chen *et al.* reported the observation of all four oxide states (not seen in this work), which is evidence of structural disorder, assuming

the same branching ratio and spin-orbit split as reported here. We estimate from their work a BE shift for the $n = 1,2,3,4$ oxide states from pure Si of +1.2, +2.5, +3.6, and +4.5 eV, respectively, which are all larger than the standard values mentioned in Sec. III. Using the same charge correction procedure as this work, Chen *et al.* found no shift between QD sizes, while they did see all samples shifting to a lower BE from the reference Si sample by ≈0.6 eV. As Chen *et al.* do not give a clear account of this shift in BE, we assume that the presence of structural disorder is to account for this phenomena.

In the studies by Kachurin *et al.* and Min *et al.*, no shift in the BE of Si 2*p* with QD diameter compared with bulk Si is reported.[8,44] A HF-etching procedure similar to ours is used in both. Kachurin *et al.* report an implantation condition that would imply the Si implant profile is embedded in a silica glass substrate and not a thermal oxide, which have different densities. In both cases, their XPS spectra show a larger concentration of Si compared to the surrounding SiO_2 matrix, which can be a function of the depth of HF etching.

To compare with Si-QDs produced by methods other than ion implantation, we note that Kim *et al.* produced an oxide layer of a varying stoichiometric ratio, from SiO_x with $x = 1.0 \rightarrow 1.6$, from substrate to surface.[49] After annealing, they report varying e-Si-QD size with depth as observed by TEM. Using Ar^+ sputtering with *in situ* XPS, a shift in the Si 2*p* is reported with depth (or QD size). However, the variation in the stoichiometry of the surrounding oxide, which plays a role in the properties of Si-QDs, is not accounted for. While Sun *et al.* reports a shift in Si 2*p* in porous Si,[50] we have noted that a porous Si system is not identical to e-Si-QDs. Finally, the work by Riabinina *et al.* considers Si-QDs created by pulsed laser deposition, which show a unique shift in the Si 2*p* peak as a function of the O pressure.[51]

A study that has been frequently cited as observation of Si 2*p* shifts due to QD size is that of van Buuren *et al.*[52] However, in this work the Si-QDs were grown on the surface by thermal vaporization, forming star-shaped islands, as opposed to the spherical QDs in this work. Furthermore, the surface coordination of a QD exposed to air and the stress on the QD due to lattice mismatch with the substrate make the system not comparable with an e-Si-QD system.

B. Suboxides and stress

The formation of suboxides is a key feature in understanding the mechanisms involved in radiative recombination for e-Si-QDs. As mentioned, our fitting procedure indicates that the only suboxide is the 3^+ state, which is at a very low concentration compared to 4^+; see Fig. 3. The majority of the 4^+ signal comes from the SiO_2 matrix. There are many studies regarding the structure of e-Si-QDs, which concentrate on the crystallinity of the QDs and the interface structure; here we talk about a selected few. It is established that e-Si-QDs exist as a pure Si diamond lattice surrounded by a suboxide layer and then by the SiO_2 matrix as shown schematically in Fig. 4. However, some debate exists about what suboxide state the intermediate layer is, which we find to be Si_2O_3. Furthermore, we can estimate the thickness of this suboxide layer by using

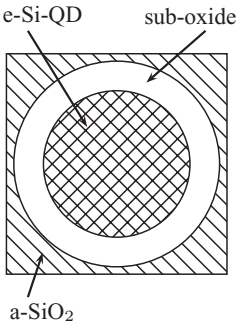

FIG. 4. Schematic representation of the e-Si-QD structure.

the relative areas for the Si^{0+} and Si^{3+} peaks given in Fig. 3. Using our results for the QD diameters (Table I), we calculate the suboxide thickness as 0.57 to 0.63 nm for the 1.55- to 1.76-nm QDs, respectively.

MD simulations performed by Djurabekova *et al.* show that the silanone bond (Si=O, oxidation state: 2^+) forms as the suboxide barrier around the e-Si-QDs, which acts to relax the stress in the system.[53] The discrepancy between their result and ours might arise from the fact that the MD simulations are performed by first removing a section of the SiO_2 matrix the size of the Si-QD, which is then placed in the matrix. The system is then annealed, which leads to the Si=O bonds as an intermediate state. One should also consider the nature of the implantation process, which creates vacancies and other defects, and in turn leads to the creation of several suboxide states.[43] Annealing after implantation causes the reformation of stoichiometric oxide with e-Si-QDs as shown in Fig. 4. Therefore, we conclude the procedure used in the MDs simulation may cause the artificial formation of Si=O bonds.

In a similar MD simulation, Soulairol *et al.* follow the same procedure; however, prior to placing the QD in the SiO_2 matrix, the matrix was subjected to several annealing cycles.[54] These cycles allow the structure factor to be very close to the given experimental values. They found that manually placing an O bond at the outer layer of the Si-QD yielded the lowest possible energy configuration and relieved stress in the Si-QDs through a Si-O-Si bridging bond (oxidation state: 1^+). Further, they concluded that no Si=O bonds form in the system; however, there is a small concentration of 3^+ oxide states.

It is important to note that as Soulairol *et al.* point out other groups do obtain the 3^+ oxide state both experimentally and from first-principle simulations (see Refs. 16 and 54). It is further noted that the 3^+ state acts to relax the stress in the system with a bond length of ≈1.8 Å. From our calculation for the suboxide thickness, we can say this layer is roughly three atomic layers thick. Therefore, we conclude that the 3^+ state is the correct suboxide state and there is no stress on the e-Si-QDs. The lack of stress in the system is discussed further in Sec. IV B 1.

Two studies regarding ion-implanted e-Si-QDs are Levitcharsky *et al.* and Nikolova *et al.*[26,33] We discussed these works briefly in Sec. II A. In these studies Ar milling is used to obtain a depth profile of the Si concentration and of the suboxide states for e-Si-QDs. It is noted that only in the case of an implantation dose of 3×10^{17} cm^{-2} does one see a

significant concentration of the 3^+ oxide state. In samples of lower dose, the concentration of the 3^+ oxide state is significantly reduced. Therefore, it is clear that implantation dose has a strong correlation with the formation of subsequent suboxide states, possibly due to the fact that Si implantation into amorphous SiO_2 preferentially sputters O by a factor of 2 : 1.[31] In addition, the Ar-milling procedure preferentially sputters O, as mentioned in Sec. II A. Therefore, we cannot accurately compare these results to ours.

Si-QDs created by PECVD have a Si/matrix interface structure that makes comparison with e-Si-QDs formed via ion implantation questionable. In the work of Dane *et al.*, the Si^{4+} is 4.3 eV above the Si^{0+} peak, which is a departure from the accepted value of 3.9 eV (see Sec. III), and the Si^{0+} peak is found to shift from bulk Si by 0.6 eV.[30] (A similar result was found for low-energy-implanted Si-QDs, which we analogously attribute to defect centers; see Sec. IV A.) These results are unlike implanted Si-QDs, which are relatively defect free, contain highly crystalline QDs, and exhibit only a single suboxide state.

1. Raman measurements

Another effect that could cause a shift in the Si 2*p* peak is a change in the bond length of Si in the nanocrystal, possibly due to stress.[50] For our QD sizes, this effect should cause a shift on the order of $\approx 1 \rightarrow 1.5$ eV, which again is not seen beyond the charging effect, in our XPS data. Furthermore, if there is stress in the system, we should be able to resolve it with Raman spectroscopy. In the Raman spectra for each of the QD samples, there is no observation of a shift in the Si Raman peak from bulk Si of 520 cm^{-1}, within experimental error. This result indicates a lack of stress on e-Si-QDs, as opposed to porous Si.[55]

C. Valence level and quantum confinement effects

In general, quantum confinement means the electron *e* and hole *h* energies in their respective bands (conduction *C* and valence *V*, respectively) gain a dimensional dependence as

$$E_{C(V)} \propto \frac{1}{m_{e(h)} D^n}; \quad n \in \mathbb{Q}^+.$$

In turn, this effect means that the energy of the gap as determined through the electronic structure has a dimensional dependence. Table I says that the magnitude of the effects of quantum confinement can vary greatly between theories. The lack of any shift in the Si 2*p* peak tells us that no shift is observed in binding energy below the Fermi level, meaning the valence level energy must also remain constant with QD size.

The valence states determined by XPS are shown in Fig. 5 for Si-ref, SiO_2-ref, and sample d. Note that the valence states are the same for all e-Si-QD samples. The DOS for sample d can be described as a convolution of the Si and SiO_2 DOS. Therefore, we take the feature around 0 eV, in Fig. 5, to be representative of the e-Si-QDs. Under this assumption, we are able to determine any shift in the valence band max (VBM). Figure 6 clearly indicates that the there is no shift in the VBM (set at $\approx$1.4 eV), as determined by taking the midpoint of the valence band edge.

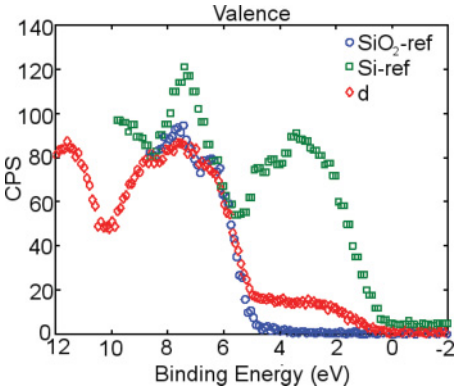

FIG. 5. (Color online) XPS counts per seconds (CPS) vs binding energy for the valence band density of states.

Quantum confinement effects should produce a shift in the VBM beyond charging. In our model,[16]

$$E_V = \frac{2(\hbar\ 3.142)^2}{D^2} \frac{1}{3.24 \times 10^{-32}\ \mathrm{eVs}^2/\mathrm{Å}^2}, \tag{4}$$

where E_V is the valence energy and *D* is the diameter of the QD. A conservative estimate, that is, using the size ranges given for Barbagiovanni *et al.* in Table I, corresponds to an additional shift of $\approx$0.25 eV, for samples a through d, within experimental error. This fact means that after charge correction an additional shift should still be present, as 0.2 eV is resolvable in VBM measurements. An even larger effect due to quantum confinement is predicted by the work of Öğüt *et al.* through pseudopotential calculations, from samples a to d of 2.1 to 2.5 eV, which is clearly not observed.[56] Furthermore, stress (see Sec. IV B 1) in the system would cause a change in the bond length, in turn changing the position of the VBM, which is also not observed.

The lack of a shift in the VBM is understood through several results presented here. As discussed in Sec. II, the samples were annealed in forming gas, which is well known to passivate dangling bonds.[22] In addition, defects introduced from the implantation process are removed through annealing, and the resulting e-Si-QDs are highly crystalline.[20,25] Henceforth, from the results of Secs. IV B and IV B 1, we conclude that the Si_2O_3 interfacial layer acts to trap free carriers. Therefore, the

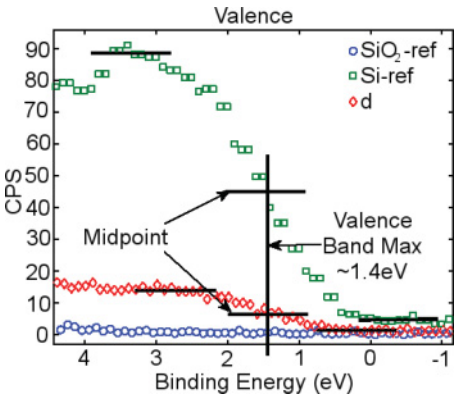

FIG. 6. (Color online) XPS counts per seconds (CPS) vs binding energy for the VBM position, determined by the midpoint method.

resulting e-Si-QDs are free from donor states, which typically cause the bending of the VBM for Si structures.[57]

As we do not see any change in the VBM, one possible conclusion is that translational symmetry is not present in the h states, that is, the kinetic term for the h is not a function of QD size. Most notably, we are able to derive this result theoretically. If we modify our theory, by removing the kinetic term for the hole from Eq. (A7), we can accurately reproduce the experimental results for the 3D confinement; see Fig. 1. Details are given in the appendix. The curve for 3D confinement e term only is given by

$$E_{\mathrm{PL}} = E_{\mathrm{Gap}}(\infty) + \frac{139.2\ \mathrm{eV}\cdot\mathrm{\AA}^2}{D^2} \quad \text{(3D confinement : e term only).} \tag{5}$$

This result is quite striking as it verifies the lack of symmetry in the h states and is more realistic than our previous model. It is important to note that we assumed the QDs to be spherical (as TEM reveals), which would imply roughly 128 atoms per QD, whereas a cubic QD would have roughly 190 atoms. In either case, the variation in QD diameters, given in Table I, is for an average size and does not correspond to a integer number of unit cells. Inasmuch as one typically performs an electronic structure calculation over an integer number of unit cells, the change in the number of atoms (QD size) nonetheless corresponds to a change in the optical properties, which implies new possible dynamics for the hole. Further analysis of these results is needed and may lead to new physics as there is not, at present, a theory that can *a priori* predict such a result.

V. CONCLUSIONS

We have demonstrated that there is no shift for an e-Si-QD in the Si 2p peak due to quantum confinement effects or bond length contraction with QD miniaturization. Initially, there is a shift in this peak due to charging: Coulombic and interface charge buildup, which is properly accounted for by charge correcting the Si 2p peak. Any change in bond length would most likely be due to stress, and our Raman measurements showed no signs of stress on the e-Si-QDs. We conclude that the lack of stress is due to suboxide formation around the e-Si-QD of Si_2O_3, which relaxes the bonds as reported by MD simulations. This fact is further seen in the VB measurements, where no shift is observed either due to quantum confinement or stress as a result of pinning by the interface layer. The lack of a shift is further explained by noting that the h states do not assume a kinetic term and using this fact in the calculations yields a result that matches with the experiment.

Our results have been compared against similar published studies, where we note that consistently e-Si-QDs do not exhibit a shift in the Si 2p level, while systems of QDs created by alternative techniques (e.g., PECVD) may or may not yield a shift. In addition, a low-energy ion implantation can yield results that differ from those of a high-energy implant. In turn, we compared our result with various models for quantum confinement and noted that models like linear combination of atomic orbitals, and some DFT calculations do not show any shift in the VB and are closer to experimental results, but they do not accurately predict the expansion of the band gap. On the other hand, our field theoretical model does accurately predict the expansion of the gap, albeit through empirical assumptions. Furthermore, these considerations indicate the need for a theory from a bottom-up approach that does not consider electrons and holes to be symmetrically equivalent. Further work is needed to properly describe the wave states of particles confined within e-Si-QDs.

Notably, we derived Eq. (5) under the "particle-in-a-box" model for quantum confinement, after taking into account results presented here, by removing the hole symmetry. This calculation is able to fit the experimental data rather well; however, assumptions needed to be made that do not accurately reflect the low-dimensional nature of a QD (i.e., the Bloch hypothesis). A further complication in our understanding is the fact that a variation of QD size yielding quite different radiative energies can occur through a minimal change in the number of QD atoms. Therefore, one may conclude that the suboxide layer and the possible dynamics of the hole play a larger role in the electronic structure and the radiative process, respectively, than first assumed. We consider these experimental results to be a firm starting point toward a complete theoretical description of e-Si-QDs. One may consider e-Si-QDs to be in an relaxed crystalline state, while the significance of a stable valence band must be included in further quantum confinement theories.

ACKNOWLEDGMENTS

We gratefully acknowledge Mark Biesinger at Surface Science Western for work on the XPS data and many valuable discussions; Jack Hendriks of the Western Tandetron Accelerator Facility for valuable help with ion implantation; Sean Shieh and Sanda Botis for help with Raman spectroscopy; and the University of Western Ontario's Nanofabrication Facility for use of facilities. Funding was provided from NSERC/CRSNG and the University of Western Ontario.

APPENDIX

In this section, we derive Eqs. (3), (4), and (5). The advantage of the formalism presented here is that it can be easily generalized, whereas our application is for the simplest possible case. We start with the general field equation for a system of interacting particles via a Coulombic interaction given by

$$\mathcal{H} = \int d^3r\,\psi^\dagger(r)\left(\frac{-\hbar^2}{2m}\nabla^2\right)\psi(r) + \frac{1}{2}\int d^3r\,d^3\acute{r}\,\psi^\dagger(r)\psi^\dagger(\acute{r})\frac{e^2}{\epsilon|r-\acute{r}|}\psi(\acute{r})\psi(r), \tag{A1}$$

where $\psi(r)$ is the field operator, ϵ is the dielectric constant of the surrounding medium, and e is the electric charge. The field operators are expanded in a two-band model for the conduction band C and the valence band V as

$$\psi^\dagger(r) = \sum_k a^\dagger_{k,i}\varphi^*_{k,i}(r), \qquad \psi(r) = \sum_k a_{k,i}\varphi_{k,i}(r) \quad (i \in C,V), \tag{A2}$$

where k represents a summation over momentum states. Electrons and holes obey Fermi statistics; therefore, the

creation and annihilation operators in Eq. (A2) are defined through the anticommutation relation

$$\{a_{k,i}, a^{\dagger}_{\acute{k},j}\} = \delta_{k\acute{k}}\delta_{ij}. \tag{A3}$$

The $\varphi_{k,i}(r)$ basis set in Eq. (A2) is expanded to reflect the use of an infinite confinement potential with normalized spherical harmonics in a Bloch basis $u_{k,i}$ as

$$\begin{aligned} \varphi_{k,i}(r) &= u_{k,i}\Psi_{nlm,i}(r,\theta,\phi), \\ \Psi_{nlm,i}(r,\theta,\phi) &= A_{nlm}j_{l,i}(kr)Y^{m}_{l,i}(\theta,\phi), \\ (A_{nlm})^2 &= \frac{2}{R^3}(j_{l+1,i}(k_{ln}R))^{-2}, \end{aligned} \tag{A4}$$

where $j_{l,i}$ is the spherical Bessel function, $Y^{m}_{l,i}$ is the spherical harmonic, n refers to the nth zero of $j_{l,i}(x_{ln})$, such that $x_{ln} = k_{ln}R$, and R is the radius of the QD. With these definitions, $\varphi_{k,i}(r)$ is properly normalized as

$$\int \varphi^{*}_{k,i}(r)\varphi_{\acute{k},j}(r)d^3r = \delta_{k\acute{k}}\delta_{ij}. \tag{A5}$$

By combining (A2) into (A1) and using (A4) with (A5), after showing that $\varphi_{k,i}(r)$ satisfies the variational principle for (A1) [$\varphi_{k,i}(r)$ are eigenfunctions], the following general expression is obtained:

$$\mathcal{H} = \mathcal{H}_{\rm el} + \mathcal{H}_{\rm h} + \mathcal{H}_{\rm el-h} + \mathcal{H}_{\rm el-el} + \mathcal{H}_{\rm h-h} + W_{\rm full}, \tag{A6}$$

where $\mathcal{H}_{\rm el}$ is the energy of the electrons, $\mathcal{H}_{\rm h}$ is the energy of the holes, $\mathcal{H}_{\rm el-h}$ is the interaction of electrons and holes, $\mathcal{H}_{\rm el-el}$ is the interaction of electrons and electrons, $\mathcal{H}_{\rm h-h}$ is the interaction of holes and holes, and $W_{\rm full}$ is the full energy of the valence band. The reader can explicitly verify the form of each term, which we do not list in full here as most terms fall out. For convenience, a change in notation is used. A destruction event of an electron in the valence band is equivalent to the creation of a hole in the valence band, etc. Therefore, define the electrons a_k to be in the conduction band and the holes b_k in the valence band. The new notation is

$$\text{holes} \left\{ \begin{array}{ll} a_{k,V} = b^{\dagger}_{k}; & a_{k,C} = a_k \\ a^{\dagger}_{k,V} = b_k; & a^{\dagger}_{k,C} = a^{\dagger}_{k} \end{array} \right\} \text{electrons.}$$

In the same manner as Eq. (A3),

$$\{b_{k,i}, b^{\dagger}_{\acute{k},j}\} = \delta_{k\acute{k}}\delta_{ij}.$$

Equation (A6) is solved in the exciton basis using the state Φ defined as an electron-hole pair above the ground state Φ_0 as

$$\begin{aligned} \Phi &= \sum_{k_1k_2} C_{k_1k_2}a^{\dagger}_{k_1}b^{\dagger}_{k_2}\Phi_V, \\ \Phi_V &= b_{k_3}b_{k_4}\ldots b_{k_N}\Phi_0. \end{aligned}$$

Expanding in low-lying k states near the band edge and solving $E_T = \langle\Phi|\mathcal{H}|\Phi\rangle$, with $\mathcal{H}$ given by (A6), we obtain

$$\begin{aligned} \langle\Phi|\,\mathcal{H}\,|\Phi\rangle = &\left(\frac{\hbar^2k^2_{ln}}{2m_c} + E_{o,C}\right) + \left(\frac{\hbar^2k^2_{ln}}{2m_V} - E_{o,V}\right) \\ &- \sum \delta_{k_1k_2}\delta_{k_3k_4}\left\{W\left(\begin{smallmatrix} k_1 & k_2 \\ C & V \end{smallmatrix} \middle| \begin{smallmatrix} k_3 & k_4 \\ V & C \end{smallmatrix}\right)\right. \\ &\left. - W\left(\begin{smallmatrix} k_2 & k_1 \\ V & C \end{smallmatrix} \middle| \begin{smallmatrix} k_3 & k_4 \\ V & C \end{smallmatrix}\right)\right\}, \end{aligned} \tag{A7}$$

with

$$\begin{aligned} &W\left(\begin{smallmatrix} k_1 & k_2 \\ j_1 & j_2 \end{smallmatrix} \middle| \begin{smallmatrix} k_3 & k_4 \\ j_3 & j_4 \end{smallmatrix}\right) \\ &\quad = \int d^3r\,d^3\acute{r}\,\varphi^{\dagger}_{k_1j_1}(r)\varphi^{\dagger}_{k_2j_2}(\acute{r})\frac{e^2}{\epsilon|r-\acute{r}|}\varphi_{k_3j_3}(\acute{r})\varphi_{k_4j_4}(r) \\ &(j_i \in C,V; \quad i = 1,2,3,4). \end{aligned} \tag{A8}$$

$W\left(\begin{smallmatrix} k_2 & k_1 \\ V & C \end{smallmatrix} \middle| \begin{smallmatrix} k_3 & k_4 \\ V & C \end{smallmatrix}\right)$, in Eq. (A7), is the exchange energy term, and $E_{o,V(C)}$ are constants. For indirect gap materials, the exciton is Wannier-like, in the limit $k \ll \frac{\pi}{a_c}$ (a_c is the lattice spacing), and we can drop the exchange term, which goes to zero very fast.

The final integral in (A7), as defined through (A8), is solved with the following set of approximations. The Bloch states are Taylor expanded into low-lying state; that is, the $k = 0$ state is diagonalized out. Next, take $l_i = 0$, $m_i = 0$, and $n_i = 1$, implying

$$\begin{aligned} Y^{0}_{0,j}(\theta,\phi) &= \frac{1}{\sqrt{4\pi}}, \\ j_{0,j}(k_{0,1}r) &= \frac{\sin(k_{0,1}r)}{k_{0,1}r}. \end{aligned} \tag{A9}$$

Let $r = R$, where R is the radius of the QD, and then $k_{0,1}R$ is the first-order zero of the Bessel function: $k_{0,1} = \frac{3.142}{R}$. Finally, take (A9) in the small wave-vector approximation, which gives

$$\begin{aligned} j_l(kr) &\simeq \frac{(kr)^l}{(2l+1)!!}, \\ A^2_{nlm} &\simeq \frac{2}{R^3}\left(\frac{(kr)^{l+1}}{(2l+3)!!}\right)^{-2}. \end{aligned} \tag{A10}$$

Equation (A7) is the most general final answer with Eqs. (A8), (A9), and (A10) for an indirect gap QD with an infinite confining spherical potential. The experiments analyzed in this work are all performed at room temperature; therefore, the Coulombic interaction given through Eq. (A8) is very weak and may be dropped.

Finally, the masses of the electrons and holes are replaced with the effective mass calculated using the DOS[58]: $m_c \rightarrow m^{*}_{c} = 1.08$ and $m_V \rightarrow m^{*}_{V} = 0.57$ and using $\epsilon = 11.8$, these definitions yield the equation, in terms of the QD diameter, D,

$$E_{\rm PL} = E_{\rm Gap}(\infty) + \frac{356.8\ \text{eV}\cdot\text{Å}^2}{D^2} \quad \text{(3D confinement)}. \tag{A11}$$

Equation (A11) is plotted in Fig. 1 and labeled "3D confinement." Equation (5) is obtained by dropping the second term in Eq. (A7), given by Eq. (4), based on the argument that hole translational symmetry is removed in a QD. Equation (5) is plotted in Fig. 1 and labeled "3D confinement: e term only." If we do the same calculation, but in one dimension, then Eq. (3) is obtained, which is plotted in Fig. 1 and labeled "1D confinement."

*ebarbagi@uwo.ca

[1] Editorial, Nature Nanotechnology **5**, 381 (2010).

[2] W. D. Heiss, ed., *Quantum Dots: A Doorway to Nanoscale Physics* (Springer, Berlin, 2005).

[3] X. Y. Lang, W. T. Zheng, and Q. Jiang, IEEE Trans. Nanotechnology **7**, 5 (2008).

[4] A. Zunger, Phys. Status Solidi B **224**, 727 (2001).

[5] J. Linnros, N. Lalic, A. Galeckas, and V. Grivickas, J. Appl. Phys. **86**, 6128 (1999).

[6] D. J. Lockwood and L. Pavesi, in *Silicon Photonics*, Vol. 94, edited by D. J. Lockwood and L. Pavesi (Springer, Berlin, 2004), pp. 1–52.

[7] V. A. Belyakov, V. A. Burdov, R. Lockwood, and A. Meldrum, in *Advances in Optical Technologies*, Vol. 279502, edited by D. Lockwood (2008), pp. 1–32.

[8] K. S. Min, K. V. Shcheglov, C. M. Yang, H. A. Atwater, M. L. Brongersma, and A. Polman, Appl. Phys. Lett. **69**, 2033 (1996).

[9] D. Kovalev, H. Heckler, M. Ben-Chorin, G. Polisski, M. Schwartzkopff, and F. Koch, Phys. Rev. Lett. **81**, 2803 (1998).

[10] A. D. Zdetsis, Rev. Adv. Mater. Sci. **11**, 56 (2006).

[11] L. E. Ramos, H. C. Weissker, J. Furthmüller, and F. Bechstedt, Phys. Status Solidi B **242**, 3053 (2005).

[12] N. B. Nguyen, C. Dufour, and S. Petit, J. Phys. Condens. Matter **20**, 455209 (2008).

[13] Z. Pu-Qin, H. Dong-Sheng, and W. Xing-Long, Chin. Phys. Lett. **22**, 1492 (2005).

[14] M. Nishida, Semicond. Sci. Technol. **21**, 443 (2006).

[15] N. C. Bacalis and A. D. Zdetsis, J. Math. Chem. **46**, 962 (2009).

[16] E. G. Barbagiovanni, L. V. Goncharova, P. J. Simpson, and N. Armstrong, in *Excitons and Plasmon Resonances in Nanostructures II*, edited by A. O. Govorov, A. L. Rogach, Z. M. Wang, J.-K. Wang, V. M. Shalaev, Mater. Res. Soc. Symp. Proc. 1208E (Warrendale, PA, 2010), p. 1208.

[17] C. Bonafos, B. Colombeau, A. Altibelli, M. Carrada, G. B. Assayag, B. Garrido, M. López, A. Pérez-Rodríguez, J. R. Morante, and A. Claverie, Nucl. Instrum. Methods Phys. Res., Sect. B **178**, 17 (2001).

[18] D. B. Tran Thoai, Y. Z. Hu, and S. W. Koch, Phys. Rev. B **42**, 11261 (1990).

[19] L. W. Wang and A. Zunger, J. Phys. Chem. **98**, 2158 (1994).

[20] C. R. Mokry, P. J. Simpson, and A. P. Knights, J. Appl. Phys. **105**, 114301 (2009).

[21] M. Molinari, H. Rinnert, M. Vergnat, and P. Weisbecker, Mater. Sci. Eng. B **101**, 186 (2003).

[22] M. López, B. Garrido, C. García, P. Pellegrino, A. Pérez-Rodríguez, J. R. Morante, C. Bonafos, M. Carrada, and A. Claverie, Appl. Phys. Lett. **80**, 1637 (2002).

[23] T. Shimizu-Iwayama, N. Kurumado, D. E. Hole, and P. D. Townsend, J. Appl. Phys. **83**, 6018 (1998).

[24] B. Garrido, M. López, O. González, A. Pérez-Rodríguez, J. R. Morante, and C. Bonafos, Appl. Phys. Lett. **77**, 3143 (2000).

[25] B. Garrido, M. López, A. Pérez-Rodríguez, C. García, P. Pellegrino, R. Ferrè, J. A. Moreno, J. R. Morante, C. Bonafos, M. Carrada, A. Claverie, J. de la Torre, and A. Souifi, Nucl. Instrum. Methods Phys. Res., Sect. B **216**, 213 (2004).

[26] L. Nikolova, R. G. Saint-Jacques, C. Dahmounea, and G. G. Ross, Surf. Coat. Technol. **203**, 2501 (2009).

[27] S. Schuppler, S. L. Friedman, M. A. Marcus, D. L. Adler, Y. H. Xie, F. M. Ross, Y. J. Chabal, T. D. Harris, L. E. Brus, W. L. Brown, E. E. Chaban, P. F. Szajowski, S. B. Christman, and P. H. Citrin, Phys. Rev. B **52**, 4910 (1995).

[28] H. Z. Song and X. M. Bao, Phys. Rev. B **55**, 6988 (1997).

[29] L. K. Pan, C. Q. Sun, B. K. Tay, T. P. Chen, and S. Li, J. Phys. Chem. B **106**, 11725 (2002).

[30] A. Dane, U. K. Demirok, A. Aydinli, and S. Suzer, J. Phys. Chem. B **110**, 1137 (2006).

[31] J. F. Ziegler, J. P. Biersack, and U. Littmark, *The Stopping and Range of Ions in Matter* (Pergamon Press, New York, 1985).

[32] N. Fairley, © Casa Software Ltd., Version 2.3.15 (2009) [http://www.casaxps.com/].

[33] V. Levitcharsky, R. G. Saint-Jacques, Y. Q. Wang, L. Nikolova, R. Smirani, and G. G. Ross, Surf. Coat. Technol. **201**, 8547 (2007).

[34] A. Hundertmark, *The Size Distribution and Photoluminescence Spectroscopy of Silicon Nanocrystals*, Master's thesis, Royal Institute of Technology, Sweden, 2008.

[35] M. L. Brongersma, A. Polman, K. S. Min, and H. A. Atwater, J. Appl. Phys. **86**, 759 (1999).

[36] J. Derr, K. Dunn, D. Riabinina, F. Martin, M. Chaker, and F. Rosei, Physica E **41**, 668 (2009).

[37] V. Ranjan, M. Kapoor, and V. A. Singh, J. Phys. Condens. Matter **14**, 6647 (2002).

[38] V. I. Klimov, C. J. Schwarza, D. W. McBranch, and C. W. White, Appl. Phys. Lett. **73**, 2603 (1998).

[39] C. Garcia, B. Garrido, P. Pellegrino, R. Ferre, J. A. Moreno, J. R. Morante, L. Pavesi, and M. Cazzanelli, Appl. Phys. Lett. **82**, 1595 (2003).

[40] H. Rinnert, M. Vergnat, and A. Burneau, J. Appl. Phys. **89**, 237 (2001).

[41] G. Ledoux, J. Gong, F. Huisken, O. Guillois, and C. Reynaud, Appl. Phys. Lett. **80**, 4834 (2002).

[42] C. Delerue, G. Allan, and M. Lannoo, Phys. Rev. B **48**, 11024 (1993).

[43] T. P. Chen, Y. Liu, C. Q. Sun, M. S. Tse, J. H. Hsieh, Y. Q. Fu, Y. C. Liu, and S. Fung, J. Phys. Chem. **108**, 16609 (2004).

[44] G. A. Kachurin, S. G. Yanovskaya, V. A. Volodin, V. G. Kesler, A. F. Leier, and M. O. Ruault, Semiconductors **36**, 647 (2002).

[45] M. L. Green, E. P. Gusev, R. Degraeve, and E. L. Garfunkel, J. Appl. Phys. **90**, 2057 (2001).

[46] O. Renault, R. Marlier, M. Gely, B. D. Salvo, T. Baron, M. Hansson, and N. T. Barrett, Appl. Phys. Lett. **87**, 163119 (2005).

[47] D. J. Miller, M. C. Biesinger, and N. S. McIntyre, Surf. Interface Anal. **33**, 299 (2002).

[48] It is worth emphasizing that the correction to the C 1*s* peak may be imperfect because it is in contact with the surface SiO_2; therefore, it may not properly account for any possible shift in the Si 2*p* peak. However, if we look at the shift in C 1*s* and Si 2*p*, we see that all peaks shift by the same amount, within experimental error; see Tables II and III. If our correction method is overcompensating for the shift in the peak, we should still expect to see differences from sample to sample.

[49] S. Kim, M. C. Kim, S. Cho, K. J. Kim, H. N. Hwang, and C. C. Hwang, Appl. Phys. Lett. **91**, 103113 (2007).

[50] C. Q. Sun, L. K. Pan, Y. Q. Fu, B. K. Tay, and S. Li, J. Phys. Chem. B **107**, 5113 (2003).

[51] D. Riabinina, C. Durand, J. Margot, M. Chaker, G. A. Botton, and F. Rosei, Phys. Rev. B **74**, 075334 (2006).

[52] T. van Buuren, L. N. Dinh, L. L. Chase, W. J. Siekhaus, and L. J. Terminello, Phys. Rev. Lett. **80**, 3803 (1998).

[53]F. Djurabekova and K. Nordlund, Phys. Rev. B **77**, 115325 (2008).
[54]R. Soulairol and F. Cleri, Solid State Sci. **12**, 163 (2010).
[55]S. M. F. Agulló-Rueda, J. D. Moreno, F. Ben-Hander, and J. M. Martínez-Duart, Thin Solid Films **401**, 306 (2001).
[56]S. Öğüt, J. R. Chelikowsky, and S. G. Louie, Phys. Rev. Lett. **79**, 1770 (1997).
[57]M. T. Björk, H. Schmid, J. Knoch, H. Riel, and W. Riess, Nature Nanotechnology **4**, 103 (2009).
[58]P. Y. Yu and M. Cardona, *Fundamentals of Semiconductors: Physical and Material Properties*, 3rd ed. (Springer, Berlin, 2001).